

---

# HYPERTRANSFORMER: MODEL GENERATION FOR SUPERVISED AND SEMI-SUPERVISED FEW-SHOT LEARNING

Andrey Zhmoginov, Mark Sandler, Max Vladymyrov

Google Research

{azhmogin, sandler, mxv}@google.com

## ABSTRACT

In this work we propose a *HyperTransformer*, a transformer-based model for few-shot learning that generates weights of a convolutional neural network (CNN) directly from support samples. Since the dependence of a small generated CNN model on a specific task is encoded by a high-capacity transformer model, we effectively decouple the complexity of the large task space from the complexity of individual tasks. Our method is particularly effective for small target CNN architectures where learning a fixed universal task-independent embedding is not optimal and better performance is attained when the information about the task can modulate all model parameters. For larger models we discover that generating the last layer alone allows us to produce competitive or better results than those obtained with state-of-the-art methods while being end-to-end differentiable. Finally, we extend our approach to a semi-supervised regime utilizing unlabeled samples in the support set and further improving few-shot performance.

## 1 INTRODUCTION

In few-shot learning, a conventional machine learning paradigm of fitting a parametric model to training data is taken to a limit of extreme data scarcity where entire categories are introduced with just one or few examples. A generic approach to solving this problem uses training data to identify parameters  $\phi$  of a *learner*  $a_\phi$  that given a small batch of examples for a particular task (called a *support* set) can solve this task on unseen data (called a *query* set).

One broad family of few-shot image classification methods frequently referred to as *metric-based learning*, relies on pretraining an embedding  $e_\phi(\cdot)$  and then using some distance in the embedding space to label query samples based on their closeness to known labeled support samples. These methods proved effective on numerous benchmarks (see Tian et al. (2020) for review and references), however the capabilities of the learner are limited by the capacity of the architecture itself, as these methods try to build a universal embedding function.

On the other hand, *optimization-based methods* such as seminal MAML algorithm (Finn et al., 2017) can fine-tune the embedding  $e_\phi$  by performing additional SGD updates on all parameters  $\phi$  of the model producing it. This partially addresses the constraints of metric-based methods by learning a new embedding for each new task. However, in many of these methods, all the knowledge extracted during training on different tasks and describing the learner  $a_\phi$  still has to “fit” into the same number of parameters as the model itself. Such limitation becomes more severe as the target models get smaller, while the richness of the task set increases.

In this paper we propose a new few-shot learning approach that allows us to decouple the complexity of the *task space* from the complexity of individual tasks. The main idea is to use the transformer model (Vaswani et al., 2017) that given a few-shot task episode generates an entire inference model by producing all model weights in a single pass. This allows us to encode the intricacies of the available training data inside the transformer model, while still producing specialized tiny models that can solve individual tasks. Reducing the size of the generated model and moving the computational overhead to the transformer-based weight generator, we can lower the cost of the inference on new

---

images. This can reduce the overall computation cost in cases where the tasks change infrequently and hence the weight generator is only used sporadically.

We start by observing that the self-attention mechanism is well suited to be an underlying mechanism for a few-shot CNN weight generator. In contrast with earlier CNN- (Zhao et al., 2020) or BiLSTM-based approaches (Ravi & Larochelle, 2017), the vanilla<sup>1</sup> transformer model is invariant to sample permutations and can handle unbalanced datasets with a varying number of samples per category. Furthermore, we demonstrate that a single-layer self-attention model can replicate a simplified gradient-descent-based learning algorithm. Using a transformer model to generate the logits layer on top of a conventionally learned embedding, we achieve competitive results on several common few-shot learning benchmarks. Varying transformer parameters we demonstrate that this high performance can be attributed to additional capacity of the transformer model that decouples its complexity from that of the generated CNN.

We then extend our method to support unlabeled samples by using a special input token that we concatenate to all unlabeled examples encoding the fact that their classes are unknown. In our experiments outlined in Section 4.3, we observe that adding unlabeled samples can significantly improve model performance. Interestingly, the full benefit of using additional data is only realized if the transformers use two or more layers. This result is consistent with the basic mechanism described in Section 3.2, where we show that a transformer model with at least two layers can encode the nearest-neighbor style algorithm that associates unlabeled samples with similar labeled examples. In essence, by training the weight generator to produce CNN models with best possible performance on a query set, we teach the transformer to utilize unlabeled samples without having to manually introduce additional optimization objectives. Our approach could be further generalized to treat partially known sample labels (when the true label is known to belong to some set of classes), but this will be the subject of the future work.

Finally, we explore the capability of our approach to generate all weights of the CNN model, adjusting both the logits layer and all intermediate layers producing the sample embedding. We show that by generating all layers we can improve both the training and test accuracies<sup>2</sup> of CNN models below a certain size. But, interestingly, generation of the logits layer alone appears to be sufficient above a certain model size threshold (see Figure 3). This threshold is expected to depend on the variability and the complexity of the training tasks.

In addition to being able to decouple the complexity of the task distribution from the complexity of individual tasks, another important advantage of our method is that it allows to do learning end-to-end without relying on complex nested gradients optimization and other meta-learning approaches, where the number of unrolls steps is large. In contrast with these methods, our optimization is done in a single loop of updates to the transformer (and feature extractor) parameters.

The paper is structured as follows. In Section 2, we discuss the few-shot learning problem setup and highlight related work. Section 3 introduces our approach, discusses the motivation for choosing an attention-based model and shows how our approach can be used to meta-learn semi-supervised learning algorithms. In Section 4, we discuss our experimental results. Finally, in Section 5, we provide concluding remarks.

## 2 PROBLEM SETUP AND RELATED WORK

### 2.1 FEW-SHOT LEARNING

The main goal of a *few-shot learning algorithm* is to use a set of training tasks  $\mathcal{T}_{\text{train}}$  for finding a *learner*  $a_\phi$  parameterized by  $\phi$  that given new task domains can train to recognize novel classes using just a few samples per each class. The learner  $a_\phi$  can be thought of as a function that maps task description  $T = \{(x_i, c_i)\}_{i=1}^{kn}$  containing  $k$  labeled input samples  $x_i$  for each of  $n$  classes, to the weights  $\theta = a_\phi(T)$  of a trained model  $f(x; \theta)$ . The parameters  $\phi$  are meta-optimized to maximize the performance of the model  $f(x; a_\phi(T_S))$  generated using a support set  $T_S$  with  $x$  drawn from a query set  $T_Q$ . Each task  $T = (T_S, T_Q)$  is randomly drawn from a space of training tasks  $\mathcal{T}_{\text{train}}$ .

---

<sup>1</sup>without attention masking or positional encodings

<sup>2</sup>As discussed in Section 4.2, HT with a high training accuracy can be a practical approach to model personalization under the assumption that real tasks come from the distribution seen at the training time.

---

Typically,  $T_S$  and  $T_Q$  are generated by first randomly choosing several distinct classes from the training set and then sampling examples without replacement from these classes to generate  $T_S$  and  $T_Q$ . In a classical “ $n$ -way- $k$ -shot” setting,  $n$  is the number of classes randomly sampled in each episode, and  $k$  is the number of samples for each class in the support set  $T_S$ .

The quality of a particular few-shot learning algorithm is typically evaluated using a separate test space of tasks  $\mathcal{T}_{\text{test}}$ . By forming  $\mathcal{T}_{\text{test}}$  from novel classes unseen at training time, we can evaluate generalization of different learners  $a_\phi$ . Best algorithms are expected to capture the structure present in the training set and to perform well on novel concepts. This structure may, for example, include certain properties of the distributions  $p_c(x)$  with  $c$  being the class label, or the presence of particular discriminative features in the tasks from  $\mathcal{T}_{\text{train}}$ .

## 2.2 RELATED WORK

Few-shot learning received a lot of attention from the deep learning community and while there are hundreds of few-shot learning methods, several common themes emerged in the past years. Here we outline several existing approaches, show how they relate to our method and discuss the prior work related to it.

**Metric-Based Learning.** One family of approaches involves mapping input samples into an embedding space and then using some nearest neighbor algorithm that relies on the computation of distances from a query sample embedding to the embedding computed using support samples with known labels. The metric used to compute the distance can either be the same for all tasks, or can be task-dependent. This family of methods includes, for example, such methods as Siamese networks (Koch et al., 2015), Matching Networks (Vinyals et al., 2016), Prototypical Networks (Snell et al., 2017), Relation Networks (Sung et al., 2018) and TADAM (Oreshkin et al., 2018). It has recently been argued (Tian et al., 2020) that methods based on building a powerful sample representation can frequently outperform numerous other approaches including many optimization-based methods. However, such approaches essentially amount to the “one-model solves all” approach and thus require larger models than needed to solve individual tasks.

**Optimization-Based Learning.** An alternative approach that can adapt the embedding to a new task is to incorporate optimization within the learning process. A variety of such methods are based on the approach called *Model-Agnostic Meta-Learning*, or MAML (Finn et al., 2017). In MAML,  $\theta = a_\phi$  is obtained by initializing a DNN at  $\theta_0 = \phi$  and then performing one or more gradient descent updates on a classification loss function  $L$ , i.e., computing  $\theta_{k+1} = \theta_k - \gamma \cdot (\partial L / \partial \theta)(T; \theta_k)$ . This approach was later refined (Antoniou et al., 2019) and built upon giving rise to Reptile (Nichol et al., 2018), LEO (Rusu et al., 2019) and others. One limitation of various MAML-inspired methods is that the knowledge about the set of training tasks  $\mathcal{T}_{\text{train}}$  is distilled into parameters  $\phi$  that have the same dimensionality as the model parameters  $\theta$ . Therefore, for a very lightweight model  $f(x; \theta)$  the capacity of the task-adaptation learner  $a_\phi$  is still limited by the size of  $\theta$ . Methods that use parameterized preconditioners that otherwise do not impact the model  $f(x; \theta)$  can alleviate this issue, but as with MAML, such methods can be difficult to train (Antoniou et al., 2019).

**Weight Modulation and Generation.** The idea of using a task specification to directly generate or modulate model weights has been previously explored in the generalized supervised learning context (Ratzlaff & Li, 2019) and in specific language models (Mahabadi et al., 2021; Tay et al., 2021; Ye & Ren, 2021). Some few-shot learning methods described above also employ this approach and use task-specific generation or modulation of the weights of the final classification model. For example, in LGM-Net (Li et al., 2019b) the matching network approach is used to generate a few layers on top of a task-agnostic embedding. Another approach abbreviated as LEO (Rusu et al., 2019) utilized a similar weight generation method to generate initial model weights from the training dataset in a few-shot learning setting, much like what is proposed in this article. However, in Rusu et al. (2019), the generated weights were also refined using several SGD steps similar to how it is done in MAML. Here we explore a similar idea, but largely inspired by the HYPERNETWORK approach (Ha et al., 2017), we instead propose to directly generate an entire task-specific CNN model. Unlike LEO, we do not rely on pre-computed embeddings for images and generate the model in a single step without additional SGD steps, which simplifies and stabilizes training.

---

**Transformers in Computer Vision and Few-Shot Learning.** Transformer models (Vaswani et al., 2017) originally proposed for natural language understanding applications, had since become a useful tool in practically every subfield of deep learning. In computer vision, transformers have recently seen an explosion of applications ranging from state-of-the-art image classification results (Dosovitskiy et al., 2021; Touvron et al., 2021) to object detection (Carion et al., 2020; Zhu et al., 2021), segmentation (Ye et al., 2019), image super-resolution (Yang et al., 2020), image generation (Chen et al., 2021) and many others. There are also several notable applications in few-shot image classification. For example, in Liu et al. (2021), the transformer model was used for generating universal representations in the multi-domain few-shot learning scenario. And closely related to our approach, in Ye et al. (2020), the authors proposed to accomplish embedding adaptation with the help of transformer models. Unlike our method that generates an entire end-to-end image classification model, this approach applied a task-dependent perturbation to an embedding generated by an independent task-agnostic feature extractor. In Gidaris & Komodakis (2018), a simplified attention-based model was used for the final layer generation.

### 3 HYPERTRANSFORMER

In this section, we describe our approach to few-shot learning that we call a HYPERTRANSFORMER (HT) and justify the choice of the self-attention mechanism as its basis.

#### 3.1 FEW-SHOT LEARNING MODEL

A learner  $a_\phi$  (as introduced in Section 2.1) is the core of a few-shot learning algorithm and in this paper, we choose  $a_\phi$  to be a transformer-based model that takes a task description  $T = \{(x_i, c_i)\}_{i=1}^{kn}$  as input and produces weights for some or all layers  $\{\theta_\ell | \ell \in [1, L]\}$  of the generated CNN model. Layer weights that are not generated are instead *learned* in the end-to-end fashion as ordinary task-agnostic variables. In other words, these learned layers are modified during the training phase and remain static during the evaluation phase (i.e. they are independent of the support set). In our experiments generated CNN models contain a set of convolutional layers and a final fully-connected logits layer. Here  $\theta_\ell$  are the parameters of the  $\ell$ -th layer and  $L$  is the total number of layers including the final logits layer (with index  $L$ ). The weights are generated layer-by-layer starting from the first layer:  $\theta_1(T) \rightarrow \theta_2(\theta_1; T) \rightarrow \dots \rightarrow \theta_L(\theta_1, \dots, \theta_{L-1}; T)$ . Here we use  $\theta_{a, \dots, b}$  as a short notation for  $(\theta_a, \theta_{a+1}, \dots, \theta_b)$ .

**Image and activation embeddings.** The weights for the layer  $\ell$  are either: (a) simply learned as a task-agnostic trainable variable, or (b) generated by the transformer that receives a concatenation of *image embeddings* and *activation embeddings* and sample labels  $c_i$ , or

$$\mathcal{I}^\ell := \left\{ \left( h_{\phi_l}^\ell(z_i^\ell), s_{\phi_s}(x_i), c_i \right) \right\}_{i=1, \dots, kn}.$$

The *activation embeddings* at layer  $\ell$  are produced by a convolutional *feature extractor*  $h_{\phi_l}^\ell(z_i^\ell)$  applied to the activations of the previous layer  $z_i^\ell := f_{\ell-1}(x_i; \theta_1, \dots, \theta_{\ell-1})$  for  $\ell > 1$  and  $z_i^1 := x_i$ . The intuition behind using the activation embeddings is that the choice of the layer weights should primarily depend on the inputs received by this layer.

The *image embeddings* are produced by a separate trainable convolutional neural network  $s_{\phi_s}(x_i)$  and are the same for all layers. Their purpose is to modulate each layer’s weight generator with a global high-level view of the sample that, unlike the activation embedding, is independent of the generated weights and is also fully shared between all layer generators.

**Encoding and decoding transformer inputs and outputs.** In the majority of our experiments, the input samples were encoded by concatenating image and activation embeddings from  $\mathcal{I}^\ell$  to trainable label embeddings  $\xi(c)$  with  $\xi : [1, n] \rightarrow \mathbb{R}^d$ . Here  $n$  is the number of classes per episode and  $d$  is a chosen size of the label encoding. Note that the class embeddings do not contain semantic information, but rather act as placeholders to differentiate between distinct classes. In addition to supervised few-shot learning, we also considered a semi-supervised scenario when some of the support samples are provided without the associated class information. Such unlabeled samples were fed into the transformer using the same general encoding approach, but we used an auxiliary

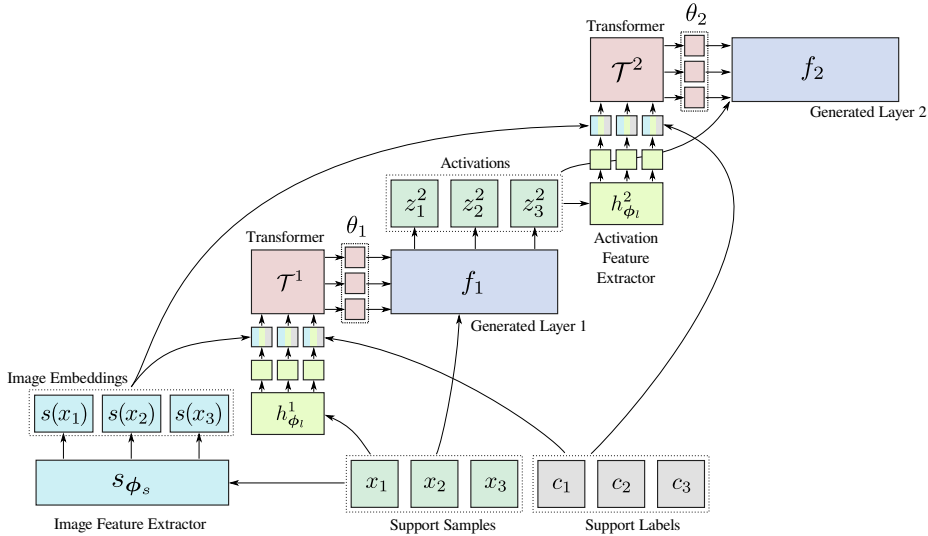


Figure 1: A diagram of our model showing the generation of two CNN layers: transformer-based weight generators receive *image embeddings*  $s_{\phi_s}(\cdot)$  and *activation embeddings*  $h_{\phi_l}(\cdot)$  along with corresponding labels  $c_i$ , and produce CNN layer weights ( $\theta_1$  and  $\theta_2$ ). After being generated, the CNN model is used to compute the loss on the query set. The gradients of this loss are then used to adjust the weights of the entire weight generation model ( $\phi_s, \phi_l$ , transformer weights).

learned “unlabeled” token  $\hat{\xi}$  in place of the label encoding  $\xi(c)$  to indicate the fact that the class of the sample is unknown.

Along with the input samples, the sequence passed to the transformer was also populated with special learnable placeholder tokens, each associated with a particular slice of the to-be-generated weight tensor. Each such token was a learnable  $d$ -dimensional vector padded with zeros to the size of the input sample token. After the entire input sequence was processed by the transformer, we read out model outputs associated with the weight slice placeholder tokens and assembled output weight slices into the final weight tensors (see Fig. 2).

In our experiments we considered two different ways of encoding  $k \times k \times n_{\text{input}} \times n_{\text{output}}$  convolutional kernels: (a) “*output allocation*” generates  $n_{\text{output}}$  tokens with weight slices of size  $k^2 \times n_{\text{input}}$  and (b) “*spatial allocation*” generates  $k^2$  weight slices of size  $n_{\text{input}} \times n_{\text{output}}$ . We show comparison results in Supplementary Materials.

**Training the model.** The weight generation model uses the support set to produce the weights of some or all CNN model layers. Then, the cross-entropy loss is computed for the query set samples that are passed through the generated CNN model. The weight generation parameters  $\phi$  (including the transformer model and image/activation feature extractor weights) are learned by optimizing this loss function using stochastic gradient descent.

### 3.2 REASONING BEHIND THE SELF-ATTENTION MECHANISM

The choice of self-attention mechanism for the weight generator is not arbitrary. One motivating reason behind this choice is that the output produced by generator with the basic self-attention is by design invariant to input permutations, i.e., permutations of samples in the training dataset. This also makes it suitable for processing unbalanced batches and batches with a variable number of samples (see Sec. 4.3). Now we show that the calculation performed by a self-attention model with properly chosen parameters can mimic basic few-shot learning algorithms further motivating its utility.

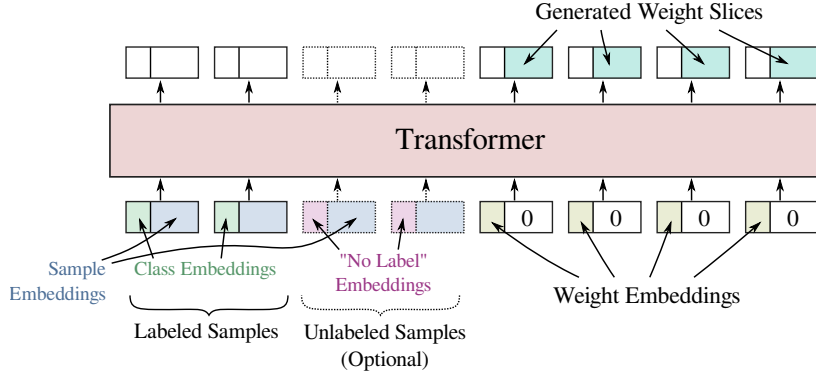


Figure 2: Structure of the tokens passed to and received from a transformer model. Both labeled and unlabeled (optional) samples can be passed to the transformer as inputs. Empty output tokens indicate ignored outputs.

**Supervised learning.** Self-attention in its rudimentary form can implement a method similar to cosine-similarity-based sample weighting encoded in the logits layer<sup>3</sup> with weights  $\mathbf{W}$ :

$$W_{i,j} \sim \sum_{m=1}^n y_i^{(m)} e_j^{(m)}, \quad (1)$$

which can also be viewed as a result of applying a single gradient descent step on the cross-entropy loss (see Appendix A). Here  $n$  is the total number of support-set samples  $\{x^{(m)} | m \in [1, n]\}$  and  $e^{(m)}, y^{(m)}$  are the embedding vector and the one-hot label corresponding to  $x^{(m)}$ .

The approach can be outlined (see more details in Appendix A) as follows. The self-attention operation receives encoded input samples  $\mathcal{I}_k = (\xi(c_k), e_k)$  and weight placeholders  $(\mu(i), 0)$  as its input. If each weight slice  $W_{i,\cdot}$  represented by a particular token  $(\mu(i), 0)$  produces a *query*  $Q_i$  that only attends to *keys*  $K_k$  corresponding<sup>4</sup> to samples  $\mathcal{I}_k$  with labels  $c_k$  matching  $i$  and the *values* of these samples are set to their embeddings  $e_k$ , then the self-attention operation will essentially average the embeddings of all samples assigned label  $i$  thus matching the first term in  $\mathbf{W}$  in equation 1.

**Semi-supervised learning.** A similar self-attention mechanism can also be designed to produce logits layer weights when the support set contains some unlabeled samples. The proposed mechanism first propagates classes of labeled samples to similar unlabeled samples. This can be achieved by a single self-attention layer choosing the *queries* and the *keys* of the samples to be proportional to their embeddings. The attention map for sample  $i$  would be defined by a softmax of  $e_i \cdot e_j$ , or in other words would be proportional to  $\exp(e_i \cdot e_j)$ . Choosing sample *values* to be proportional to the class tokens, we can then propagate a class of a labeled sample  $e_j$  to a nearby unlabeled sample with embedding  $e_i$ , for which  $e_i \cdot e_j$  is sufficiently large. If the self-attention module is “residual”, i.e., the output of the self-attention operation is added to the original input, like it is done in the transformer model, then this additive update would essentially “mark” an unlabeled sample by the propagated class (albeit this term might have a small norm). The second self-attention layer can then be designed similarly to the supervised case. If label embeddings are orthogonal, then even a small component of a class embedding propagated to an unlabeled sample can be sufficient for a weight slice to attend to it thus adding its embedding to the final weight (resulting in the averaging of embeddings of both labeled and proper unlabeled examples).

## 4 EXPERIMENTS

In this section, we present HYPERTRANSFORMER (HT) experimental results and discuss the implications of our empirical findings.

<sup>3</sup>here we assume that the embeddings  $e$  are unbiased, i.e.,  $\langle e_i \rangle = 0$

<sup>4</sup>in other words, the self-attention layer should match tokens  $(\mu(i), \dots)$ .

Table 1: Comparison of HT with MAML++ on models of different sizes and different datasets: (a) 20-way OMNIGLOT and (b) 5-way MINIIMAGENET. Results for MAML++ were obtained using GitHub code accompanying Antoniou et al. (2019), those marked with  $\dagger$  are from Antoniou et al. (2019). HT outperforms MAML++ on many few-shot tasks. Accuracy confidence intervals: OMNIGLOT – between 0.1% and 0.3%, MINIIMAGENET – between 0.2% and 0.5%.

Approach	1-shot (channels)					5-shot (channels)				
	8	16	32	48	64	8	16	32	48	64
<b>OMNIGLOT:</b>										
- MAML++	81.4	88.6	<b>95.6</b>	<b>95.8</b>	<b>97.7</b> $\dagger$	83.2	94.9	<b>98.6</b>	<b>98.8</b>	<b>99.3</b> $\dagger$
- HT	<b>87.2</b>	<b>93.7</b>	<b>95.5</b>	<b>95.7</b>	96.2	<b>94.7</b>	<b>98.0</b>	<b>98.6</b>	<b>98.8</b>	98.8
<b>MINI:</b>										
- MAML++	43.9	46.6	49.4	52.2 $\dagger$	–	<b>59.0</b>	<b>64.6</b>	66.8	<b>68.3</b> $\dagger$	–
- HT	<b>45.5</b>	<b>50.2</b>	<b>53.8</b>	<b>55.1</b>	–	58.5	63.8	<b>67.1</b>	<b>68.1</b>	–

#### 4.1 DATASETS AND SETUP

**Datasets.** For our experiments, we chose several most widely used few-shot datasets including OMNIGLOT, MINIIMAGENET and TIEREDIMAGENET. MINIIMAGENET contains a relatively small set of labels and is arguably the simplest to overfit to. Because of this and since in many recent publications MINIIMAGENET was replaced with a larger TIEREDIMAGENET dataset, we conduct many of our experiments and ablation studies using OMNIGLOT and TIEREDIMAGENET.

**Models.** HYPERTRANSFORMER can in principle generate arbitrarily large weight tensors by producing low-dimensional embeddings that can then be fed into another trainable model to generate the entire weight tensors. In this work, however, we limit our experiments to HT models that generate weight tensor slices encoding individual output channels directly. For the target models we focus on 4-layer CNN architectures identical to those used in MAML++ and numerous other papers. More precisely, we used a sequence of four  $3 \times 3$  convolutional layers with the same number of output channels followed by batch normalization (BN) layers, nonlinearities and max-pooling stride-2 layers. All BN variables were learned and not generated. Experiments with generated BN variables did not show much difference with this simpler approach. Generating larger architectures such as RESNET and WIDERESNET will be the subject of our future work.

#### 4.2 SUPERVISED RESULTS WITH LOGITS LAYER GENERATION

As discussed in Section 3.2, using a simple self-attention mechanism to generate the CNN logits layer can be a basis of a simple few-shot learning algorithm. Motivated by this observation, in our first experiments, we compared the proposed HT approach with MAML++ on OMNIGLOT and MINIIMAGENET datasets (see Table 1) with HT limited to generating only the final fully-connected logits layer.

In our experiments, the dimensionality of the activation embedding was chosen to be the same as the number of model channels and the image embedding had a dimension of 32 regardless of the model size. The image feature extractor was a simple 4-layer convolutional model with batch normalization and stride-2  $3 \times 3$  convolutional kernels. The activation feature extractors were two-layer convolutional models with outputs of both layers averaged over the spatial dimensions and concatenated to produce the final activation embedding. For all tasks except 5-shot MINIIMAGENET our transformer had 3 layers, used a simple sequence of encoder layers (Figure 2) and used the “output allocation” of weight slices (Section 3.1). Experiments with the encoder-decoder transformer architecture can be found in Appendix D. The 5-shot MINIIMAGENET results presented in Table 1 were obtained with a simplified transformer model that had 1 layer, and did not have the final fully-connected layer and nonlinearity. This proved necessary for reducing model overfitting of this smaller dataset. Other model parameters are described in detail in Appendix B.

Results obtained with our method in a few-shot setting (see Table 1) are frequently better than MAML++ results, especially on smaller models, which can be attributed to parameter disentanglement between the weight generator and the CNN model. While the improvement over MAML++

Table 2: Comparison of MINIIMAGENET and TIEREDIMAGENET 1-shot (1-S) and 5-shot (5-S) 5-way results for HT (underlined) and other widely known methods with a 64-64-64-64 model including (Tian et al., 2020): Matching Networks (Vinyals et al., 2016), IMP (Allen et al., 2019), Prototypical Networks (Snell et al., 2017), TAML (Jamal & Qi, 2019), SAML (Hao et al., 2019), GCR (Li et al., 2019a), KTN (Peng et al., 2019), PARN (Wu et al., 2019), Predicting Parameters from Activations (Qiao et al., 2018), Relation Net (Sung et al., 2018), MELR (Fei et al., 2021). We also include results for CNNs with fewer channels (“-32” for 32-channel models, etc.).

MINIIMAGENET						TIEREDIMAGENET		
Method	1-S	5-S	Method	1-S	5-S	Method	1-S	5-S
HT	54.1	68.5	HT-48	<b>55.1</b>	68.1	HT-32	<b>52.7</b>	<b>69.9</b>
MN	43.6	55.3	SAML	52.2	66.5	MAML-32	51.7	<b>70.3</b>
IMP	49.2	64.7	GCR	53.2	<b>72.3</b>	HT	<b>56.1</b>	<b>73.3</b>
PN	49.4	68.2	KTN	54.6	71.2	PN	53.3	72.7
MELR	<b>55.4</b>	<b>72.3</b>	PARN	<b>55.2</b>	71.6	MELR	<b>56.4</b>	<b>73.2</b>
TAML	51.8	66.1	PPA	54.5	67.9	RN	54.5	71.3

gets smaller with the growing size of the generated CNN, our results on MINIIMAGENET and TIEREDIMAGENET appear to be comparable to those obtained with numerous other methods (see Table 2). Discussion of additional comparisons to LGM-Net (Li et al., 2019b) and LEO (Rusu et al., 2019) using a different setup (which is why they could not be included in Table 2) and showing an almost identical performance can be found in Appendix C.

While the learned HT model could perform a relatively simple calculation on high-dimensional sample embeddings, perhaps not too different from that in equation 1, our brief analysis of the parameters space (see Appendix D) shows that using simpler 1-layer transformers leads to a modest decrease of the test accuracy and a greater drop in the training accuracy for smaller models. However, in our experiments with 5-shot MINIIMAGENET dataset, which is generally more prone to overfitting, we observed that increasing the transformer model complexity improves the model training accuracy (on episodes that only use classes seen at the training time), but the test accuracy relying on classes unseen at the training time, generally degrades. We also observed that the results in Table 1 could be improved even further by increasing the embedding sizes (see Appendix D), but we did not pursue an exhaustive optimization in the parameter space.

It is worth noting that overfitting characterized by a good performance on tasks composed of seen categories, but poor generalization to unseen categories, may still have practical applications. Specifically, if the actual task relies on classes seen at the training time, we can generate an accurate model customized to a particular task in a single pass without having to perform any SGD steps to fine-tune the model. This is useful if, for example, the client model needs to be adjusted to a particular set of known classes most widely used by this client. We also anticipate that with more complex data augmentations and additional synthetic tasks, more complex transformer-based models can further improve their performance on the test set and a deeper analysis of such techniques will be the subject of our future work.

#### 4.3 SEMI-SUPERVISED RESULTS

In our approach, the weight generation model is trained by optimizing the loss calculated on the query set and therefore any additional information about the task, including unlabeled samples, can be provided as a part of the support set to the weight generator without having to alter the optimization objective. This allows us to tackle a semi-supervised few-shot learning problem without making any substantial changes to the model or the training approach. In our implementation, we simply added unlabeled samples into the support set and marked them with an auxiliary learned “unlabeled” token  $\hat{\xi}$  in place of the label encoding  $\xi(c)$ .

Since OMNIGLOT is typically characterized by very high accuracies in the 97%-99% range, we conducted all our experiments with TIEREDIMAGENET. As shown in Table 3, adding unlabeled samples results in a substantial increase of the final test accuracy. Furthermore, notice that the model achieves its best performance when the number of transformer layers is greater than one.

---

Table 3: Test accuracy on TIEREDIMAGENET of supervised 1-shot and 5-shot models and semi-supervised 1-shot models with  $u$  additional unlabeled samples per class. The weight generation transformer model uses  $L_T$  encoder layers. Notice a performance improvement of semi-supervised learning over the 1-shot supervised results. Accuracy is seen to grow with the number of unlabeled samples and the maximum accuracy is reached when the encoder has at least two layers.

$(u, L_T)$	1-shot	5-shot	(2, 3)	(4, 1)	(4, 2)	(4, 3)	(9, 3)
Accuracy	56.0	69.9	58.3	56.6	59.9	59.9	61.5

This is consistent with the basic mechanism discussed in Section 3.2 that required two self-attention layers to function.

It is worth noticing that adding more unlabeled samples into the support set makes our model more difficult to train and it gets stuck producing CNNs with essentially random outputs. Our solution was to introduce unlabeled samples incrementally during training. This was implemented by masking out some unlabeled samples in the beginning of the training and then gradually reducing the masking probability over time. In our experiments, we linearly interpolated the probability of ignoring an unlabeled sample from 0.7 to 0.0 in half the training steps.

#### 4.4 GENERATING ADDITIONAL MODEL LAYERS

We demonstrated that HT model can outperform MAML++ on common few-shot learning datasets by generating just the last logits layer of the CNN model. But is it advantageous to be generating additional CNN layers (ultimately fully utilizing the capability of the HT model)?

We approached this question by conducting experiments, in which all or some layers were generated, while the remaining layers were learned as task-agnostic variables (usually the first few layers of the CNN). Our experimental results demonstrated a significant performance improvement due to the generation of the convolutional layers in addition to the CNN logits layer, but only for CNN models below a particular size. For OMNIGLOT dataset, we saw that both training and test accuracies for a 4-channel and a 6-channel CNNs increased with the number of generated layers (see Fig. 3 and Table 4 in Appendix) and using more complex transformer models with 2 or more encoder layers improved both training and test accuracies of fully-generated CNN models of this size (see Appendix D). However, as the size of the model increased and reached 8 channels, generating the last logits layer alone proved to be sufficient for getting the best results on OMNIGLOT and TIEREDIMAGENET. By separately training an ‘‘oracle’’ CNN model using all available data for a random set of  $n$  classes, we observed the gap between the training accuracy of the generated model and the *oracle* model (see Fig. 3), indicating that the transformer does not fully capture the dependence of the optimal CNN model weights on the support set samples. A hypothetical weight generator reaching maximum training accuracy could, in principle, memorize all training images being able to associate them with corresponding classes and then generate an optimal CNN model for a particular set of classes in the episode matching ‘‘oracle’’ model performance.

The positive effect of generating convolutional layers can also be observed in shallow models with large convolutional kernels and large strides where the model performance can be much more sensitive to a proper choice of model weights. For example, in a 16-channel model with two convolutional kernels of size 9 and the stride of 4, the overall test accuracy for a model generating only the final convolutional layer was about 1% lower than the accuracies of the models generating at least one additional convolutional filter. We also speculate that as the complexity of the task increases, generating some or all intermediate network layers should become more important for achieving optimal performance. Verifying this hypothesis and understanding the ‘‘boundary’’ in the model space between two regimes where a static backbone is sufficient or not will be the subject of our future work.

## 5 CONCLUSIONS

In this work, we proposed a *HyperTransformer* (HT), a novel transformer-based model that generates all weights of a CNN model directly from a few-shot support set. This approach allows us to use

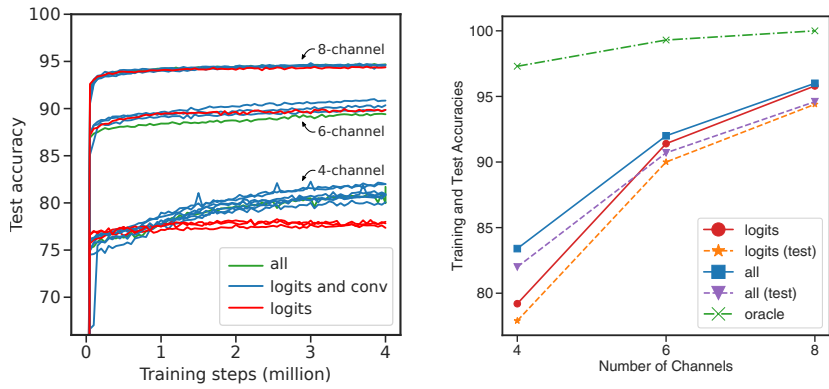


Figure 3: **(Left)** Test accuracies for the generated 4-, 6- and 8-channel CNN models on the 5-shot-20-way OMNIGLOT task. Models with only the last logits layer generated (*red*) are characterized by lower test accuracies compared to the models with some or all convolutional layers also being generated (*blue, green*). Similar plot for TIEREDIMAGE NET can be found in Appendix (Fig. 13). **(Right)** 5-shot-20-way OMNIGLOT training/test accuracies (separate run) as a function of the CNN model complexity: only the final logits layer being generated (*logits*), all layers being generated (*all*), training the model on all available samples for a random set of few classes (*oracle*). A model that generates CNN weights by memorizing all samples (being able to determine their classes) and also memorizing optimal trained weights for any selection of classes would reach the *oracle* accuracy, but would not generalize.

a high-capacity model for encoding task-dependent variations in the weights of a smaller model. We demonstrate that generating the last logits layer alone, the transformer-based weight generator beats or matches performance of multiple traditional learning methods on several few-shot benchmarks. More importantly, we showed that HT can be straightforwardly extended to handle unlabeled samples that might be present in the support set and our experiments demonstrate a considerable few-shot performance improvement in the presence of unlabeled data. Finally, we explore the impact of the transformer-encoded model diversity in CNN models of different sizes. We use HT to generate some or all convolutional kernels and biases and show that for sufficiently small models, adjusting all model parameters further improves their few-shot learning performance.

## ACKNOWLEDGEMENTS

We would like to thank Azalia Mirhoseini, David Ha, Bill Mark, Luke Metz, Raviteja Vemulapalli, Philip Mansfield, and Nolan Miller for insightful discussions.

## REFERENCES

Kelsey R. Allen, Evan Shelhamer, Hanul Shin, and Joshua B. Tenenbaum. Infinite mixture prototypes for few-shot learning. In Kamalika Chaudhuri and Ruslan Salakhutdinov (eds.), *Proceedings of the 36th International Conference on Machine Learning, ICML 2019, 9-15 June 2019, Long Beach, California, USA*, volume 97 of *Proceedings of Machine Learning Research*, pp. 232–241. PMLR, 2019.

Antreas Antoniou, Harrison Edwards, and Amos J. Storkey. How to train your MAML. In *7th International Conference on Learning Representations, ICLR 2019, New Orleans, LA, USA, May 6-9, 2019*. OpenReview.net, 2019.

Nicolas Carion, Francisco Massa, Gabriel Synnaeve, Nicolas Usunier, Alexander Kirillov, and Sergey Zagoruyko. End-to-end object detection with transformers. In Andrea Vedaldi, Horst Bischof, Thomas Brox, and Jan-Michael Frahm (eds.), *Computer Vision - ECCV 2020 - 16th European Conference on Computer Vision, Glasgow, UK, September 12-18, 2020, Proceedings, Part I*, volume 12345 of *Lecture Notes in Computer Science*, pp. 42–57. Springer, 2020.

---

*European Conference, Glasgow, UK, August 23-28, 2020, Proceedings, Part I*, volume 12346 of *Lecture Notes in Computer Science*, pp. 213–229. Springer, 2020.

Hanting Chen, Yunhe Wang, Tianyu Guo, Chang Xu, Yiping Deng, Zhenhua Liu, Siwei Ma, Chun-jing Xu, Chao Xu, and Wen Gao. Pre-trained image processing transformer. In *IEEE Conference on Computer Vision and Pattern Recognition, CVPR 2021, virtual, June 19-25, 2021*, pp. 12299–12310. Computer Vision Foundation / IEEE, 2021.

Alexey Dosovitskiy, Lucas Beyer, Alexander Kolesnikov, Dirk Weissenborn, Xiaohua Zhai, Thomas Unterthiner, Mostafa Dehghani, Matthias Minderer, Georg Heigold, Sylvain Gelly, Jakob Uszkoreit, and Neil Houlsby. An image is worth 16x16 words: Transformers for image recognition at scale. In *9th International Conference on Learning Representations, ICLR 2021, Virtual Event, Austria, May 3-7, 2021*, 2021.

Nanyi Fei, Zhiwu Lu, Tao Xiang, and Songfang Huang. MELR: meta-learning via modeling episode-level relationships for few-shot learning. In *9th International Conference on Learning Representations, ICLR 2021, Virtual Event, Austria, May 3-7, 2021*. OpenReview.net, 2021.

Chelsea Finn, Pieter Abbeel, and Sergey Levine. Model-agnostic meta-learning for fast adaptation of deep networks. In Doina Precup and Yee Whye Teh (eds.), *Proceedings of the 34th International Conference on Machine Learning*, volume 70 of *Proceedings of Machine Learning Research*, pp. 1126–1135. PMLR, 06–11 Aug 2017.

Spyros Gidaris and Nikos Komodakis. Dynamic few-shot visual learning without forgetting. In *2018 IEEE Conference on Computer Vision and Pattern Recognition, CVPR 2018, Salt Lake City, UT, USA, June 18-22, 2018*, pp. 4367–4375. IEEE Computer Society, 2018. doi: 10.1109/CVPR.2018.00459.

David Ha, Andrew M. Dai, and Quoc V. Le. HyperNetworks. In *5th International Conference on Learning Representations, ICLR 2017, Toulon, France, April 24-26, 2017, Conference Track Proceedings*, 2017.

Fusheng Hao, Fengxiang He, Jun Cheng, Lei Wang, Jianzhong Cao, and Dacheng Tao. Collect and select: Semantic alignment metric learning for few-shot learning. In *2019 IEEE/CVF International Conference on Computer Vision, ICCV 2019, Seoul, Korea (South), October 27 - November 2, 2019*, pp. 8459–8468. IEEE, 2019. doi: 10.1109/ICCV.2019.00855.

Muhammad Abdullah Jamal and Guo-Jun Qi. Task agnostic meta-learning for few-shot learning. In *IEEE Conference on Computer Vision and Pattern Recognition, CVPR 2019, Long Beach, CA, USA, June 16-20, 2019*, pp. 11719–11727. Computer Vision Foundation / IEEE, 2019. doi: 10.1109/CVPR.2019.01199.

Gregory Koch, Richard Zemel, Ruslan Salakhutdinov, et al. Siamese neural networks for one-shot image recognition. In *ICML deep learning workshop*, volume 2. Lille, 2015.

Aoxue Li, Tiange Luo, Tao Xiang, Weiran Huang, and Liwei Wang. Few-shot learning with global class representations. In *2019 IEEE/CVF International Conference on Computer Vision, ICCV 2019, Seoul, Korea (South), October 27 - November 2, 2019*, pp. 9714–9723. IEEE, 2019a. doi: 10.1109/ICCV.2019.00981.

Huai-Yu Li, Weiming Dong, Xing Mei, Chongyang Ma, Feiyue Huang, and Bao-Gang Hu. Lgm-net: Learning to generate matching networks for few-shot learning. In Kamalika Chaudhuri and Ruslan Salakhutdinov (eds.), *Proceedings of the 36th International Conference on Machine Learning, ICML 2019, 9-15 June 2019, Long Beach, California, USA*, volume 97 of *Proceedings of Machine Learning Research*, pp. 3825–3834. PMLR, 2019b.

Lu Liu, William L. Hamilton, Guodong Long, Jing Jiang, and Hugo Larochelle. A universal representation transformer layer for few-shot image classification. In *9th International Conference on Learning Representations, ICLR 2021, Virtual Event, Austria, May 3-7, 2021*. OpenReview.net, 2021.

Chongyang Ma. LGM-Net. <https://github.com/likesiwell/LGM-Net>, 2019.

---

Rabeeh Karimi Mahabadi, Sebastian Ruder, Mostafa Dehghani, and James Henderson. Parameter-efficient multi-task fine-tuning for transformers via shared hypernetworks. In Chengqing Zong, Fei Xia, Wenjie Li, and Roberto Navigli (eds.), *Proceedings of the 59th Annual Meeting of the Association for Computational Linguistics and the 11th International Joint Conference on Natural Language Processing, ACL/IJCNLP 2021, (Volume 1: Long Papers), Virtual Event, August 1-6, 2021*, pp. 565–576. Association for Computational Linguistics, 2021. doi: 10.18653/v1/2021.acl-long.47.

Alex Nichol, Joshua Achiam, and John Schulman. On first-order meta-learning algorithms. *CoRR*, abs/1803.02999, 2018.

Boris N. Oreshkin, Pau Rodríguez López, and Alexandre Lacoste. TADAM: task dependent adaptive metric for improved few-shot learning. In Samy Bengio, Hanna M. Wallach, Hugo Larochelle, Kristen Grauman, Nicolò Cesa-Bianchi, and Roman Garnett (eds.), *Advances in Neural Information Processing Systems 31: Annual Conference on Neural Information Processing Systems 2018, NeurIPS 2018, December 3-8, 2018, Montréal, Canada*, pp. 719–729, 2018.

Zhimao Peng, Zechao Li, Junge Zhang, Yan Li, Guo-Jun Qi, and Jinhui Tang. Few-shot image recognition with knowledge transfer. In *2019 IEEE/CVF International Conference on Computer Vision, ICCV 2019, Seoul, Korea (South), October 27 - November 2, 2019*, pp. 441–449. IEEE, 2019. doi: 10.1109/ICCV.2019.00053.

Siyuan Qiao, Chenxi Liu, Wei Shen, and Alan L. Yuille. Few-shot image recognition by predicting parameters from activations. In *2018 IEEE Conference on Computer Vision and Pattern Recognition, CVPR 2018, Salt Lake City, UT, USA, June 18-22, 2018*, pp. 7229–7238. Computer Vision Foundation / IEEE Computer Society, 2018. doi: 10.1109/CVPR.2018.00755.

Neale Ratzlaff and Fuxin Li. Hypergan: A generative model for diverse, performant neural networks. In Kamalika Chaudhuri and Ruslan Salakhutdinov (eds.), *Proceedings of the 36th International Conference on Machine Learning, ICML 2019, 9-15 June 2019, Long Beach, California, USA*, volume 97 of *Proceedings of Machine Learning Research*, pp. 5361–5369. PMLR, 2019.

Sachin Ravi and Hugo Larochelle. Optimization as a model for few-shot learning. In *5th International Conference on Learning Representations, ICLR 2017, Toulon, France, April 24-26, 2017, Conference Track Proceedings*. OpenReview.net, 2017.

Andrei A. Rusu, Dushyant Rao, Jakub Sygnowski, Oriol Vinyals, Razvan Pascanu, Simon Osindero, and Raia Hadsell. Meta-learning with latent embedding optimization. In *7th International Conference on Learning Representations, ICLR 2019, New Orleans, LA, USA, May 6-9, 2019*, 2019.

Jake Snell, Kevin Swersky, and Richard S. Zemel. Prototypical networks for few-shot learning. In Isabelle Guyon, Ulrike von Luxburg, Samy Bengio, Hanna M. Wallach, Rob Fergus, S. V. N. Vishwanathan, and Roman Garnett (eds.), *Advances in Neural Information Processing Systems 30: Annual Conference on Neural Information Processing Systems 2017, December 4-9, 2017, Long Beach, CA, USA*, pp. 4077–4087, 2017.

Flood Sung, Yongxin Yang, Li Zhang, Tao Xiang, Philip H. S. Torr, and Timothy M. Hospedales. Learning to compare: Relation network for few-shot learning. In *2018 IEEE Conference on Computer Vision and Pattern Recognition, CVPR 2018, Salt Lake City, UT, USA, June 18-22, 2018*, pp. 1199–1208. IEEE Computer Society, 2018. doi: 10.1109/CVPR.2018.00131.

Yi Tay, Zhe Zhao, Dara Bahri, Donald Metzler, and Da-Cheng Juan. Hypergrid transformers: Towards A single model for multiple tasks. In *9th International Conference on Learning Representations, ICLR 2021, Virtual Event, Austria, May 3-7, 2021*. OpenReview.net, 2021.

Yonglong Tian, Yue Wang, Dilip Krishnan, Joshua B. Tenenbaum, and Phillip Isola. Rethinking few-shot image classification: A good embedding is all you need? In Andrea Vedaldi, Horst Bischof, Thomas Brox, and Jan-Michael Frahm (eds.), *Computer Vision - ECCV 2020 - 16th European Conference, Glasgow, UK, August 23-28, 2020, Proceedings, Part XIV*, volume 12359 of *Lecture Notes in Computer Science*, pp. 266–282. Springer, 2020. doi: 10.1007/978-3-030-58568-6\\_16.

---

Hugo Touvron, Matthieu Cord, Matthijs Douze, Francisco Massa, Alexandre Sablayrolles, and Hervé Jégou. Training data-efficient image transformers & distillation through attention. In Marina Meila and Tong Zhang (eds.), *Proceedings of the 38th International Conference on Machine Learning, ICML 2021, 18-24 July 2021, Virtual Event*, volume 139 of *Proceedings of Machine Learning Research*, pp. 10347–10357. PMLR, 2021.

Ashish Vaswani, Noam Shazeer, Niki Parmar, Jakob Uszkoreit, Llion Jones, Aidan N. Gomez, Łukasz Kaiser, and Illia Polosukhin. Attention is all you need. In Isabelle Guyon, Ulrike von Luxburg, Samy Bengio, Hanna M. Wallach, Rob Fergus, S. V. N. Vishwanathan, and Roman Garnett (eds.), *Advances in Neural Information Processing Systems 30: Annual Conference on Neural Information Processing Systems 2017, December 4-9, 2017, Long Beach, CA, USA*, pp. 5998–6008, 2017.

Oriol Vinyals, Charles Blundell, Tim Lillicrap, Koray Kavukcuoglu, and Daan Wierstra. Matching networks for one shot learning. In Daniel D. Lee, Masashi Sugiyama, Ulrike von Luxburg, Isabelle Guyon, and Roman Garnett (eds.), *Advances in Neural Information Processing Systems 29: Annual Conference on Neural Information Processing Systems 2016, December 5-10, 2016, Barcelona, Spain*, pp. 3630–3638, 2016.

Ziyang Wu, Yuwei Li, Lihua Guo, and Kui Jia. PARN: position-aware relation networks for few-shot learning. In *2019 IEEE/CVF International Conference on Computer Vision, ICCV 2019, Seoul, Korea (South), October 27 - November 2, 2019*, pp. 6658–6666. IEEE, 2019. doi: 10.1109/ICCV.2019.00676.

Fuzhi Yang, Huan Yang, Jianlong Fu, Hongtao Lu, and Baining Guo. Learning texture transformer network for image super-resolution. In *2020 IEEE/CVF Conference on Computer Vision and Pattern Recognition, CVPR 2020, Seattle, WA, USA, June 13-19, 2020*, pp. 5790–5799. Computer Vision Foundation / IEEE, 2020. doi: 10.1109/CVPR42600.2020.00583.

Han-Jia Ye, Hexiang Hu, De-Chuan Zhan, and Fei Sha. Few-shot learning via embedding adaptation with set-to-set functions. In *2020 IEEE/CVF Conference on Computer Vision and Pattern Recognition, CVPR 2020, Seattle, WA, USA, June 13-19, 2020*, pp. 8805–8814. IEEE, 2020. doi: 10.1109/CVPR42600.2020.00883.

Linwei Ye, Mrigank Rochan, Zhi Liu, and Yang Wang. Cross-modal self-attention network for referring image segmentation. In *IEEE Conference on Computer Vision and Pattern Recognition, CVPR 2019, Long Beach, CA, USA, June 16-20, 2019*, pp. 10502–10511. Computer Vision Foundation / IEEE, 2019. doi: 10.1109/CVPR.2019.01075.

Qinyuan Ye and Xiang Ren. Learning to generate task-specific adapters from task description. In Chengqing Zong, Fei Xia, Wenjie Li, and Roberto Navigli (eds.), *Proceedings of the 59th Annual Meeting of the Association for Computational Linguistics and the 11th International Joint Conference on Natural Language Processing, ACL/IJCNLP 2021, (Volume 2: Short Papers), Virtual Event, August 1-6, 2021*, pp. 646–653. Association for Computational Linguistics, 2021. doi: 10.18653/v1/2021.acl-short.82.

Dominic Zhao, Johannes von Oswald, Sejin Kobayashi, João Sacramento, and Benjamin F Grewe. Meta-learning via hypernetworks. 2020.

Xizhou Zhu, Weijie Su, Lewei Lu, Bin Li, Xiaogang Wang, and Jifeng Dai. Deformable DETR: deformable transformers for end-to-end object detection. In *9th International Conference on Learning Representations, ICLR 2021, Virtual Event, Austria, May 3-7, 2021*. OpenReview.net, 2021.

---

## A EXAMPLE OF A SELF-ATTENTION MECHANISM FOR SUPERVISED LEARNING

Self-attention in its rudimentary form can implement a cosine-similarity-based sample weighting, which can also be viewed as a simple 1-step MAML-like learning algorithm. This can be seen by considering a simple classification model

$$f(x; \theta) = s(\mathbf{W} \mathbf{e}(x; \phi) + \mathbf{b})$$

with  $\theta = (\mathbf{W}, \mathbf{b}, \phi)$ , where  $\mathbf{e}(x; \phi)$  is the embedding and  $s(\cdot)$  is a softmax function. MAML algorithm identifies such initial weights  $\theta_0$  that given any task  $T$  just a few gradient descent steps with respect to the loss  $\mathcal{L}_T$  starting at  $\theta_0$  bring the model towards a task-specific local optimum of  $\mathcal{L}_T$ .

Notice that if any label assignment in the training tasks is equally likely, it is natural for  $f(x; \theta_0)$  to not prefer any particular label over the others. Guided by this, let us choose  $\mathbf{W}_0$  and  $\mathbf{b}_0$  that are *label-independent*. Substituting  $\theta = \theta_0 + \delta\theta$  into  $f(x; \theta)$ , we obtain

$$f_\ell(x; \theta) = f_\ell(x; \theta_0) + s'_\ell(\cdot)(\delta\mathbf{W}_\ell \mathbf{e}(x; \phi_0) + \delta\mathbf{b}_\ell + \mathbf{W}_{0,\ell} \mathbf{e}'(x; \phi_0) \delta\phi) + O(\delta\theta^2),$$

where  $\ell$  is the label index and  $\delta\theta = (\delta\mathbf{W}, \delta\mathbf{b}, \delta\phi)$ . We see that the lowest-order label-dependent correction to  $f_\ell(x; \theta_0)$  is given simply by  $s'_\ell(\cdot)(\delta\mathbf{W}_\ell \mathbf{e}(x; \phi_0) + \delta\mathbf{b}_\ell)$ . In other words, in the lowest-order, the model only adjusts the final logits layer to adapt the pretrained embedding  $\mathbf{e}(x; \phi_0)$  to a new task. It is then easy to calculate that for a simple softmax cross-entropy loss, a single step of the gradient descent results in the following logits weight and bias updates:

$$\delta W_{ij} = \frac{\gamma}{n} \sum_{m=1}^n \left( y_i^{(m)} - \frac{1}{|C|} \right) e_j(x^{(m)}; \phi_0), \quad \delta b_i = \frac{\gamma}{n} \sum_{m=1}^n \left( y_i^{(m)} - \frac{1}{|C|} \right). \quad (2)$$

Here  $\gamma$  is the learning rate,  $n$  is the total number of support-set samples,  $|C|$  is the number of classes and  $\mathbf{y}^{(m)}$  is the one-hot label corresponding to  $x^{(m)}$ .

Now consider a self-attention module generating the last logits layer and acting on a sequence of processed input samples<sup>5</sup>  $\mathcal{I}^L = \{(\xi(c_i), h_{\phi_l}(e_i))\}_{i=1,\dots,n}$  and weight placeholders  $\mathcal{W}^L := \{(\mu(k), 0)\}_{k=1,\dots,|C|}$ , where  $|C|$  is the number of classes and also the number of weight slices of  $\mathbf{W}$  if each slice corresponds to an output layer channel. The output of a simple self-attention module for the weight slice with index  $i$  is then given by:

$$Z^{-1} \sum_{m=1}^n e^{\mathbf{Q}(\mathcal{W}_i^L) \cdot \mathbf{K}_I(\mathcal{I}_m^L)} \mathbf{V}_I(\mathcal{I}_m^L) + Z^{-1} \sum_{m=1}^{N_w} e^{\mathbf{Q}(\mathcal{W}_i^L) \cdot \mathbf{K}_W(\mathcal{W}_m^L)} \mathbf{V}_W(\mathcal{W}_m^L), \quad (3)$$

where  $Z := \sum_{m=1}^n e^{\mathbf{Q}(\mathcal{W}_i^L) \cdot \mathbf{K}_I(\mathcal{I}_m^L)} + \sum_{m=1}^{N_w} e^{\mathbf{Q}(\mathcal{W}_i^L) \cdot \mathbf{K}_W(\mathcal{W}_m^L)}$ . It is easy to see that with a proper choice of query and key matrices attending only to prepended  $\xi$  and  $\mu$  tokens, the second term in equation 3 can be made negligible, while  $\mathbf{Q}(\mathcal{W}_i^L) \cdot \mathbf{K}_I(\mathcal{I}_m^L)$  can make the softmax function only attend to those components of  $\mathbf{V}_I$  that correspond to samples with label  $i$ . Choosing  $\mathbf{V}_I(\mathcal{I}_m^L)$  to be proportional to  $\mathbf{e}_m$ , we can then recover the first term in  $\delta\mathbf{W}$  in equation 2. The second term in  $\delta\mathbf{W}$  can be produced, for example, with the help of a second head that generates identical attention weights for all samples, thus summing up their embeddings.

## B MODEL PARAMETERS

Here we provide additional information about the model parameters used in our experiments.

**Image augmentations and feature extractor parameters.** For OMNIGLOT dataset, we used the same image augmentations that were originally proposed in MAML. For MINIIMAGENET and TIEREDIMAGENET datasets, however, we used ImageNet-style image augmentations including horizontal image flipping, random color augmentations and random image cropping. This helped us to avoid model overfitting on the MINIIMAGENET dataset and possibly on TIEREDIMAGENET.

---

<sup>5</sup>here we use only activation features  $h_{\phi_l}(e_i)$  of the sample embedding vectors  $e_i$

---

The dimensionality  $d$  of the label encoding  $\xi$  and weight slice encoding  $\mu$  was typically set to 32. Increasing  $d$  up to the maximum number of weight slices plus the number of per-episode labels, would allow the model to fully disentangle examples for different labels and different weight slices, but can also make the model train slower.

**Transformer parameters.** Since the weight tensors of each layer are generally different, our per-layer transformers were also different. The key, query and value dimensions of the transformer were chosen to be equal to a pre-defined fraction  $\nu$  of the input embedding size, which in turn was a function of the label, image and activation embedding sizes and the sizes of the weight slices. The inner dimension of the final fully-connected layer in the transformer was also chosen using the same approach. In our MINIIMAGENET and TIEREDIMAGENET experiments,  $\nu$  was chosen to be 0.5 and in OMNIGLOT experiments, we used  $\nu = 1$ . Each transformer typically contained 2 or 3 encoder layers and used 2 or 8 heads for OMNIGLOT and MINIIMAGENET, TIEREDIMAGENET, correspondingly.

**Learning schedule.** In all our experiments, we used gradient descent optimizer with a learning rate in the 0.01 to 0.02 range. Our early experiments with more advanced optimizers were unstable. We used a learning rate decay schedule, in which we reduced the learning rate by a factor of 0.95 every  $10^5$  learning steps.

## C ADDITIONAL SUPERVISED EXPERIMENTS

While the advantage of decoupling parameters of the weight generator and the generated CNN model is expected to vanish with the growing CNN model size, we compared our approach to two other methods, LGM-Net (Li et al., 2019b) and LEO (Rusu et al., 2019), to verify that our approach can match their performance on sufficiently large models.

For our comparison with the LGM-Net method, we used the same image augmentation technique that was used in Li et al. (2019b) where it was applied both at the training and the evaluation stages (Ma, 2019). We also used the same CNN architecture with 4 learned 64-channel convolutional layers followed by two generated convolutional layers and the final logits layer. In our weight generator, we used 2-layer transformers with activation feature extractors that relied on 48-channel convolutional layers and did not use any image embeddings. We trained our model in the end-to-end fashion on the MINIIMAGENET 1-shot-5-way task and obtained a test accuracy of  $69.3\% \pm 0.3\%$  almost identical to the 69.1% accuracy reported in Li et al. (2019b).

We also carried out a comparison with LEO by using our method to generate a fully-connected layer on top of the TIEREDIMAGENET embeddings pre-computed with a WideResNet-28 model employed by Rusu et al. (2019). For our experiments, we used a simpler 1-layer transformer model with 2 heads that did not have the final fully-connected layer and nonlinearity. We also used  $L_2$  regularization of the generated fully-connected weights setting the regularization weight to  $10^{-3}$ . As a result of training this model, we obtained  $66.2\% \pm 0.2\%$  and  $81.6\% \pm 0.2\%$  test accuracies on the 1-shot-5-way and 5-shot-5-way TIEREDIMAGENET tasks correspondingly. These results are almost identical to 66.3% and 81.4% accuracies reported in Rusu et al. (2019).

## D DEPENDENCE ON PARAMETERS AND ABLATION STUDIES

Most of our parameter explorations were conducted for OMNIGLOT dataset. We chose a 16-channel model trained on a 1-shot-20-way OMNIGLOT task as an example of a model, for which just the logits layer generation was sufficient. We also chose a 4-channel model trained on a 5-shot-20-way OMNIGLOT task for the role of a model, for which generation of all convolutional layers proved to be beneficial. Figures 5 and 6 show comparison of training and test accuracies on OMNIGLOT for different parameter values for these two models. Here we only used two independent runs for each parameter value, which did not allow us to sufficiently reduce the statistical error. Despite of this, in the following, we try to highlight a few notable parameter dependencies. Note here that in some experiments with particularly large embedding or model sizes, training progressed beyond the target number of steps and there could also be overfitting for very large models.

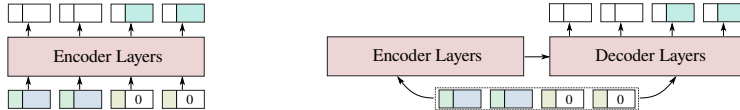


Figure 4: Two transformer-based approaches to weight generation studied in our experiments: only encoder layers (left), encoder and decoder layers on the same input sequence (right).

**Number of transformer layers.** Increasing the number of transformer layers is seen to be particularly important in the 4-channel model. The 16-channel model also demonstrates the benefit of using 1 vs 2 transformer layers, but the performance appears to degrade when we use 3 transformer layers.

**Activation embedding dimension.** Particularly, small activation embeddings can be seen to hurt the performance in both models, while using larger activation embeddings appears to be advantageous in most cases except for the 32-dimensional activation embeddings in the 4-channel model.

**Class embedding dimension.** Particularly low embedding dimension of 16 can be seen to hurt the performance of both models.

**Number of transformer heads.** Increasing the number of transformer heads leads to performance degradation in the 16-channel model, but does not have a pronounced effect in the 4-channel model.

**Image embedding dimensions.** Removing the image embedding, or using an 8-dimensional embedding can be seen to hurt the performance in both cases of the 4- and 16-channel models.

**Transformer architecture.** While the majority of our experiments were conducted with a sequence of transformer encoder layers, we also experimented with an alternative weight generation approach, where both encoder and decoder transformer layers were employed (see Fig. 4). Our experiments with both architectures suggest that the role of the decoder is pronounced, but very different in two models: in the 16-channel model, the presence of the decoder increases the model performance, while in the 4-channel model, it leads to accuracy degradation.

**Inner transformer embedding sizes.** Varying the  $\nu$  parameter for different components of the transformer model (key/query pair, value and inner fully-connect layer size), we quantify their importance on the model performance. Using very low  $\nu$  for the value dimension hurts performance of both models. The effect of key/query and inner dimensions can be distinctly seen only in the 4-channel model, where using  $\nu = 1$  or  $\nu = 1.5$  appears to produce the best results.

**Weight allocation approach.** Our experiments with the “spatial” weight allocation in 4- and 16-channel models showed slightly inferior performance (both accuracies dropping by about 0.2% to 0.4% in both experiments) compared to that obtained with the “output” weight allocation method.

## E ATTENTION MAPS OF LEARNED TRANSFORMER MODELS

We visualized the attention maps of several transformer-based models that we used for CNN layer generation. Figure 7 shows attention maps for a 2-layer 4-channel CNN network generated using a 1-head 1-layer transformer on MINIIMAGENET (labeled samples are sorted in the order of their episode labels). Attention map for the final logits layer (“CNN Layer 3”) is seen to exhibit a “stairways” pattern indicating that a weight slice  $W_{c,:}$  for episode label  $c$  is generated by attending to all samples except for those with label  $c$ . This is reminiscent of the supervised learning mechanism outlined in Sec. 3.2. While the proposed mechanism would attend to all samples with label  $c$  and average their embeddings, another alternative is to average embeddings of samples with other labels and then invert the result. We hypothesize that the trained transformer performs a similar calculation with additional learned transformer parameters, which may be seen to result in mild fluctuations of the attention to different input samples.

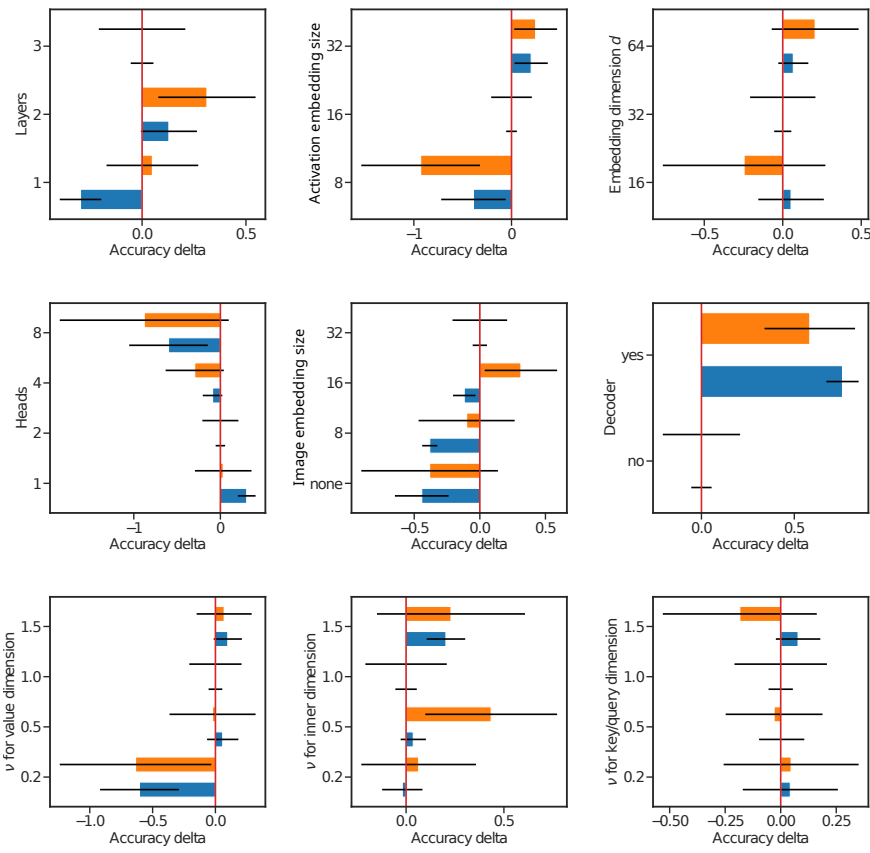


Figure 5: Change of the training (blue) and test (orange) accuracies on 1-shot-20-way OMNIGLOT task for a 16-channel model relative to the *base* configuration with 3-layer transformer, 16-dimensional activation embedding,  $\nu = 1.0$ ,  $d = 32$ , 2 heads and 32-dimensional image embedding. Approximate confidence intervals are shown.

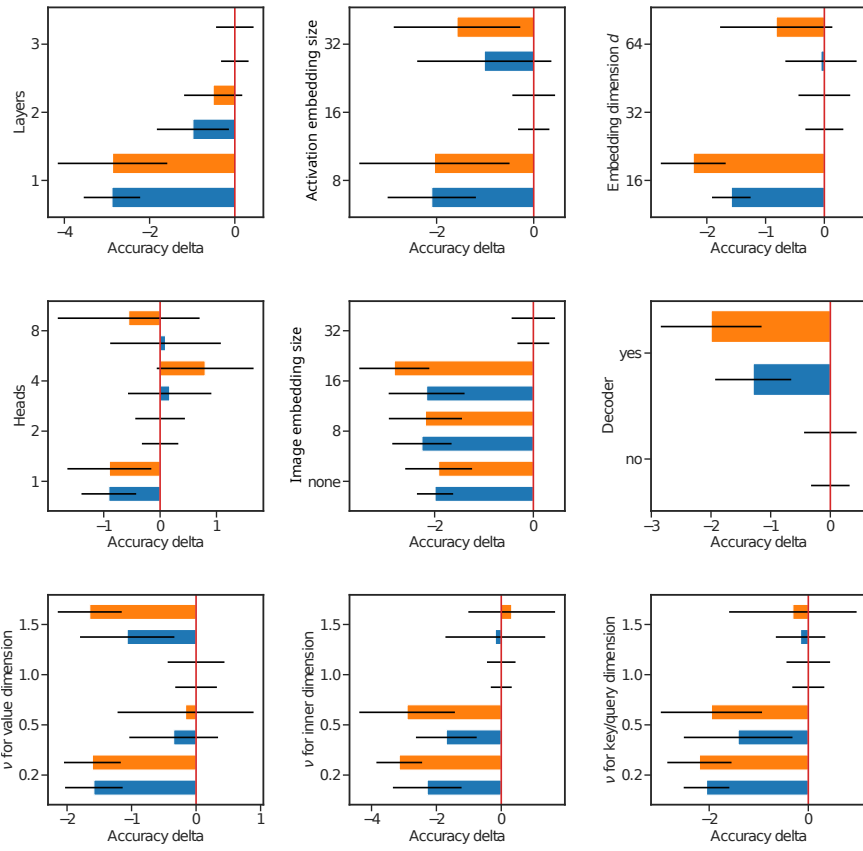


Figure 6: Change of the training (blue) and test (orange) accuracies on 5-shot-20-way OMNIGLOT task for a 4-channel model relative to the *base* configuration with 3-layer transformer, 16-dimensional activation embedding,  $\nu = 1.0$ ,  $d = 32$ , 2 heads and 32-dimensional image embedding. Approximate confidence intervals are shown.

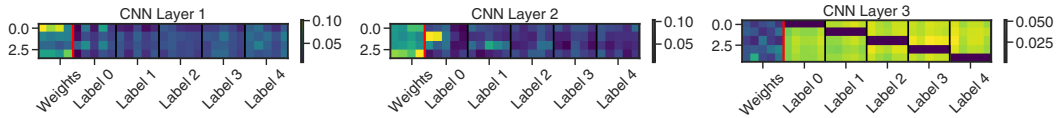


Figure 7: Learned attention maps for 2-layer 4-channel CNN network generated with 1 head, 1 layer transformer for 5-shot MINIIMAGENET.

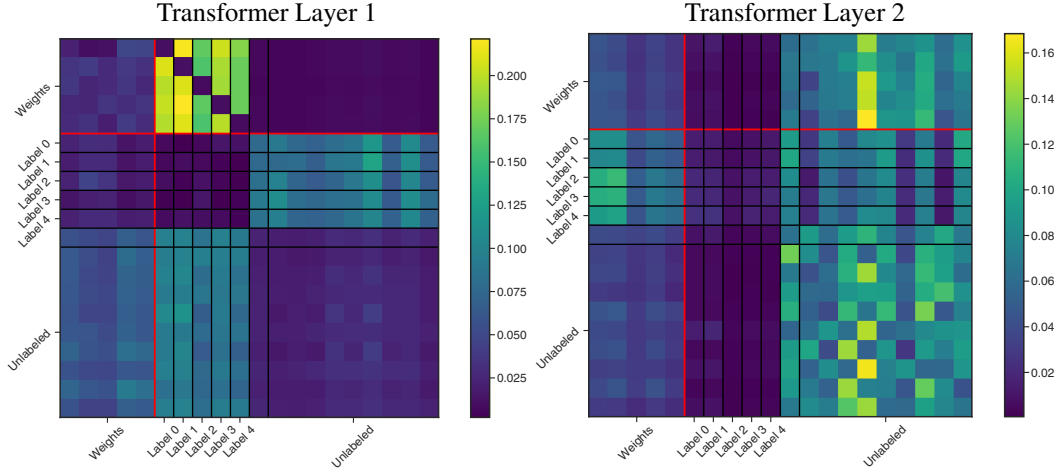


Figure 8: Learned attention maps for 4-layer 8-channel CNN network generated with 1-head, 2-layer transformer for 5-shot TIEREDIMAGENET with additional unsupervised samples (2 per class). Only the last layer of CNN is generated.

The attention maps for a semi-supervised learning problem with a 2-layer transformer is shown in Figure 8. One thing to notice is that a mechanism similar to the one described above appears to be used in the first transformer layer, where weight slices  $W_{c,\cdot}$  attend to all labeled samples with labels  $c_i \neq c$ . At the same time, unlabeled samples can be seen to attend to labeled samples in layer 1 (see ‘‘Unlabeled’’ rows and ‘‘Label ...’’ columns) and the weight slices in layer 2 then attend to the updated unlabeled sample tokens (see ‘‘Weights’’ rows and ‘‘Unlabeled’’ columns in the second layer). This additional pathway connecting labeled samples to unlabeled samples and finally to the logits layer weights is again reminiscent of the simplistic semi-supervised learning mechanism outlined in Sec. 3.2.

The exact details of these calculations and the generation of intermediate convolutional layers is generally much more difficult to interpret just from the attention maps and a more careful analysis of the trained model is necessary to draw the final conclusions.

## F VISUALIZATION OF THE GENERATED CNN WEIGHTS.

Figures 9 and 10 show the examples of the CNN kernels that are generated by a single-head, 1-layer transformer for a simple 2-layer CNN model with  $9 \times 9$  stride-4 kernels. Different figures correspond to different approaches to re-assembling the weights from the generated slices: using ‘‘output’’ allocation or ‘‘spatial’’ allocation (see Section 3.1 in the main text for more information). Notice that ‘‘spatial’’ weight allocation produces more homogeneous kernels for the first layer when compared to the ‘‘output’’ allocation. In both figures we show the difference of the final generated kernels for 3 variants: model with both layers generated, one generated and one trained and both trained.

Trained layers are always fixed for the inference for all the episodes, but the generated layers vary, albeit not significantly. In Figures 11 and 12 we show the generated kernels for two different episodes and, on the right, the difference between them. It appears that the generated convolutional kernel change within 10 – 15% from episode to episode.

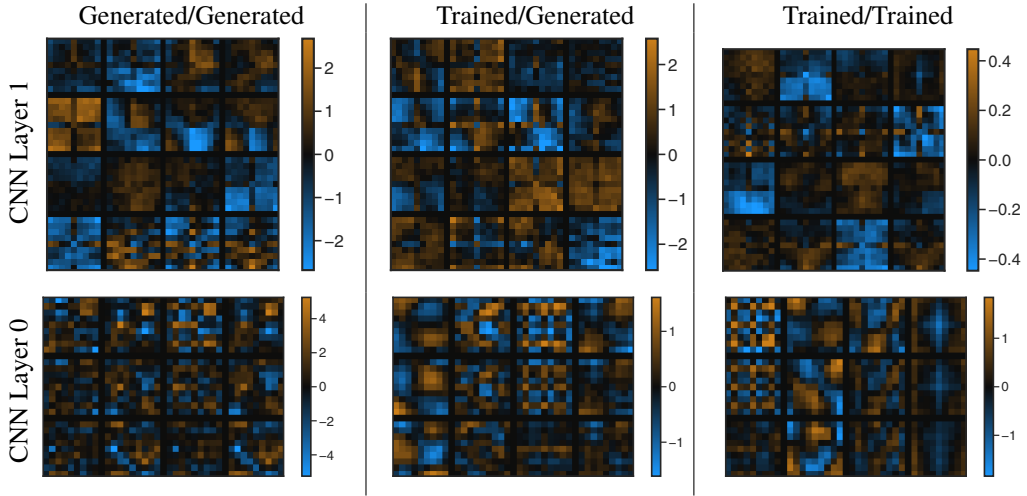


Figure 9: Visualizing convolutional kernels for a 2-layer network with a  $9 \times 9$  CNN kernel size and stride of 4 trained on MINIIMAGENET. Each column shows 1 model with two layers and fully-connected head that is always generated by the transformer. *Left*: both CNN layers are generated, *center*: first CNN layer is trained, second is generated, *right*: both CNN layers are trained. Layer weight allocation: “output”.

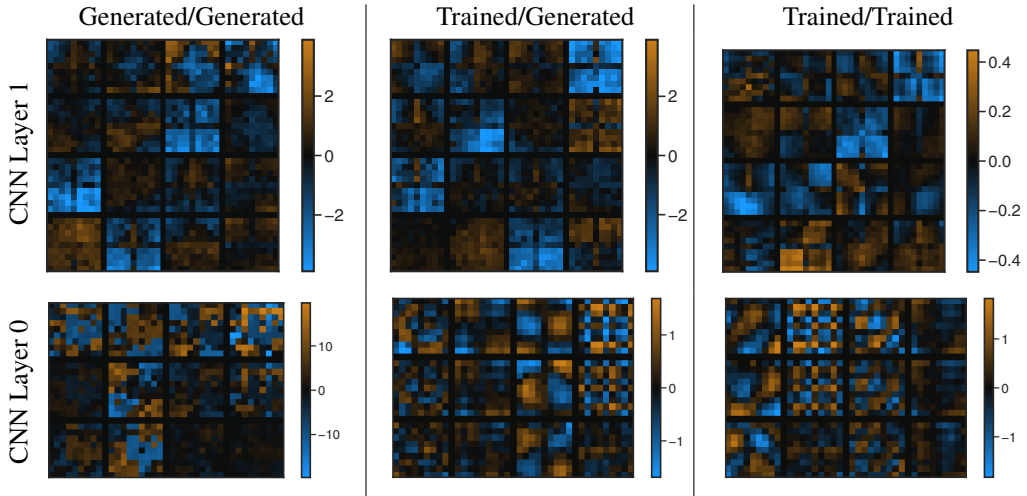


Figure 10: Visualizing convolutional kernels for a 2-layer network with a  $9 \times 9$  CNN kernel size and stride of 4 trained on MINIIMAGENET. Each column shows 1 model with two layers and fully-connected head that is always generated by the transformer. *Left*: both CNN layers are generated, *center*: first CNN layer is trained, second is generated, *right*: both CNN layers are trained. Layer weight allocation: “spatial”.

## G ADDITIONAL TABLES AND FIGURES

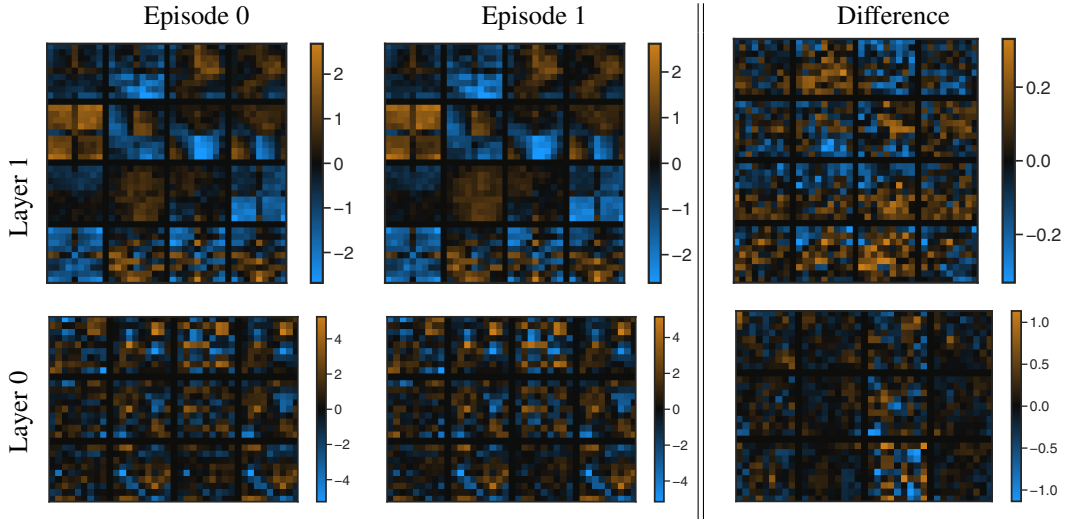


Figure 11: Visualizing generated convolutional kernels in a 2-layer model for two different episodes. *Left two plots*: kernels for two random episodes of 5 classes, *right*: the difference in generated kernels for two episodes. Layer weight allocation: “output”.

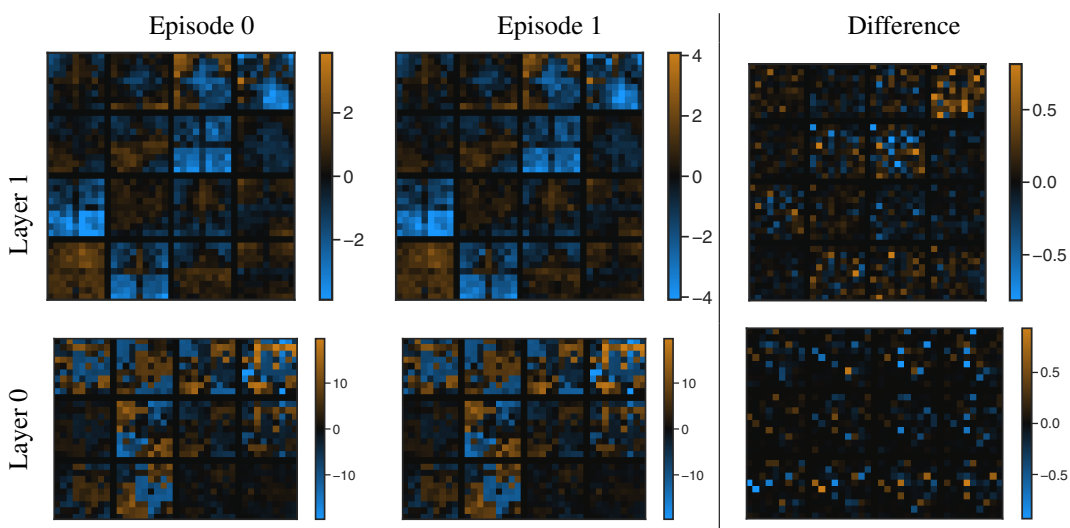


Figure 12: Visualizing generated convolutional kernels in a 2-layer model for two different episodes. *Left two plots*: kernels for two random episodes of 5 classes, *right*: the difference in generated kernels for two episodes. Layer weight allocation: “spatial”.

Table 4: Average model test and training accuracies on OMNIGLOT (separated by a slash) for the models of different sizes. “Logits” row shows accuracies for the model with only the fully-connected logits layer generated from the support set. It can be interpreted as a method based on a learned embedding. “All” row reports accuracies of the models with some or all convolutional layers being generated. We were not able to see a statistically significant evidence of an advantage of generating more than one convolutional layers.

	4-channel	6-channel	8-channel
<b>Logits</b>	77.9 / 79.2	90.0 / 91.4	94.4 / 95.8
<b>All</b>	82.0 / 83.4	90.7 / 92.0	94.6 / 96.0

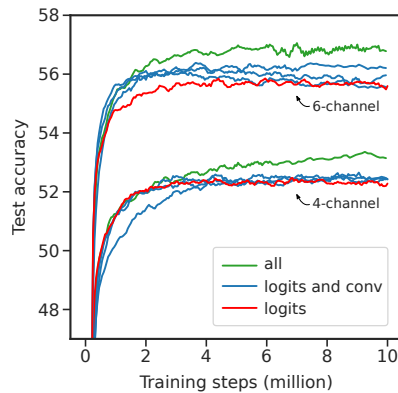


Figure 13: Test accuracies for the generated 4-channel and 6-channel CNN models on the 5-shot-5-way TIEREDIMAGENET task. Models with only the last logits layer generated (*red*) are characterized by the lower test accuracies compared to the models with some or all convolutional layers also being generated (*blue* and *green*).